



Short communication

Real-time estimation of lead-acid battery parameters: A dynamic data-driven approach



Yue Li, Zheng Shen, Asok Ray*, Christopher D. Rahn

Department of Mechanical and Nuclear Engineering, Pennsylvania State University, University Park 16802, USA

HIGHLIGHTS

- Estimation of State of charge (SOC) and State of health (SOH) in lead-acid batteries.
- Algorithm development based on symbolic dynamic filtering for feature extraction and k-NN for pattern classification.
- Validation on experimental data.

ARTICLE INFO

Article history:

Received 18 February 2014

Received in revised form

18 June 2014

Accepted 18 June 2014

Available online 7 July 2014

Keywords:

State of charge

State of health

Lead-acid battery

Symbolic dynamic filtering

k-NN regression

ABSTRACT

This short paper presents a recently reported dynamic data-driven method, Symbolic Dynamic Filtering (SDF), for real-time estimation of the state-of-health (SOH) and state-of-charge (SOC) in lead-acid batteries, as an alternative to model-based analysis techniques. In particular, SOC estimation relies on a k-NN regression algorithm while SOH estimation is obtained from the divergence between extracted features. The results show that the proposed data-driven method successfully distinguishes battery voltage responses under different SOC and SOH situations.

© 2014 Elsevier B.V. All rights reserved.

1. Introduction

Lead-acid batteries provide low-cost energy storage with high power density and operational safety. Consequently, large lead-acid battery packs are increasingly being used in vehicles, renewable energy applications, power backup systems, and the smart grid. Applications requiring large and dynamic power demands (e.g., plug-in electric vehicles and hybrid locomotives) use real-time estimates of the state of health (SOH) and the state of charge (SOC) to efficiently allocate power and energy within battery packs and between other prime movers such as internal combustion engines. Accurate SOC estimates mitigate the risk of the battery system being over-charged and over-discharged; similarly, reliable SOH estimates enhance preventive maintenance and life cycle cost through recharging or replacement of battery units.

The battery SOC and SOH can be estimated from the available current and voltage measurements at reasonable sampling rates (e.g.,

~1 Hz for experiments in this paper) based on a simplified model of the cell electrochemistry. This approach results in estimates that explicitly related to the geometric, material, and electrochemical characteristics of the underlying model. A variety of parameter estimation tools (e.g., system identification, minimum variance, and linear least squares) have been applied to lead-acid [1] and lithium-ion [2] batteries.

This paper proposes a dynamic data-driven approach for SOC and SOH estimation of the lead-acid batteries as an alternative to a model-based approach. The proposed estimation method is built upon the concept of symbolic dynamic filtering (SDF) [3] that has been successfully applied in a variety of physical processes for anomaly detection [4] and pattern recognition [5]. The major advantages of the data-driven parameter estimation method, presented in this short paper, are delineated below.

- The proposed method of battery parameter estimation is capable of real-time execution on in-situ computers (e.g., at sensor nodes of individual batteries).
- There is no requirement for a detailed knowledge of the battery electrochemistry and its internal dynamics.

* Corresponding author.

E-mail addresses: yol5214@psu.edu (Y. Li), zus120@psu.edu (Z. Shen), axr2@psu.edu (A. Ray), cdrahn@psu.edu (C.D. Rahn).

2. Battery state parameters

This section introduces standard definitions of pertinent battery parameters, at a given ambient temperature [6].

Definition 2.1. (Battery capacity) The capacity $C(t)$ of a battery at time t is its maximum charge (in units of ampere-hours) that can be drawn from its fully charged condition at a rate $C(t)/30$ (in units of amperes).

Definition 2.2. (SOH) Let a new battery be put into service at time t_0 . The state of health SOH(t) of the (possibly used) battery at the current time t , where $t \geq t_0$, is defined to be the ratio of the battery capacities at time epochs t and t_0 , i.e.,

$$\text{SOH}(t) = \frac{C(t)}{C(t_0)} \quad \forall t \geq t_0 \quad (1)$$

Definition 2.3. (DOD and SOC) Let a battery be fully charged at time t and let $I(\tau)$ be the applied current (in units of amperes) at time τ . Then, depth of discharge (DOD) and state of charge (SOC) at time $t + \Delta t$ are respectively defined as

$$\text{DOD}(t + \Delta t) = \frac{1}{C(t)} \int_t^{t+\Delta t} I(\tau) d\tau, \Delta t \geq 0 \quad (2)$$

$$\text{SOC}(t + \Delta t) = 1 - \text{DOD}(t + \Delta t), \Delta t \geq 0 \quad (3)$$

Remark 2.1. It is noted that $\text{SOH} \in [0,1]$ and $\text{SOC} \in [0,1]$ for all time $t \geq t_0$, where t_0 is the time of putting a new battery into service.

The current practice of SOH estimation includes battery capacity measurement, battery impedance measurement, and coup de fouet methods [7]. Capacity measurement is a slow process as it requires full discharge to $\text{SOC} = 0$ followed by a full charge to $\text{SOC} = 1$. Impedance measurement employs dedicated hardware and/or software to directly measure either DC or AC resistance of the battery [8,9]. The battery impedance also increases as the battery ages and the measured impedance can be correlated to SOH. Coup de fouet [7], [10] is observed in Lead-Acid batteries that have been fully charged, rested, and then pulse discharged. During the first discharge pulse, the voltage dips and then increases and levels off at a plateau voltage, followed by a steady rate of decrease. The voltage dip or undershoot has been empirically shown to be proportional to SOH of the cell [11], [12]. In this work, the capacity measurement method has been used to calibrate the SOH at different stages of battery life.

There are several existing methods for SOC estimation, which include ampere-hour counting, measurements of electrolyte's physical properties, and open-circuit voltage testing. Ampere-hour counting requires an accurate current measurement and the SOC estimate is computed from Definition 2.3. The electrolyte in lead-acid batteries plays an important role in the charge and discharge reactions. The linear relationship between the acid concentration and SOC can be used to determine the latter; similarly, the open circuit voltage varies monotonically with SOC. In this paper, ampere-hour counting has been used to compute the SOC for the experimental work.

3. Symbolization of time series

This section briefly describes the underlying concept of symbolic dynamic filtering (SDF) upon which the proposed data-driven tool of battery parameter estimation is constructed. SDF encodes the behavior of (possibly nonlinear) dynamical systems from the observed time series by symbolization and construction of state machines (i.e., probabilistic finite state automata (PFSA)) [3]. This is followed by computation of the state probability vectors that are representatives of the evolving statistical characteristics of the battery's dynamical system.

Symbolization is achieved by partitioning the time series data into a mutually exclusive and exhaustive set of finitely many segments. In this paper, the maximum-entropy partitioning (MEP) [13] has been adopted to construct the symbol alphabet Σ and to generate symbol sequences, where the information-rich regions of the data set are partitioned finer and those with sparse information are partitioned coarser to maximize the Shannon entropy of the generated symbol sequence from the reference data set. As seen at the upper left hand corner plot of Fig. 1, each segment is labeled by a unique symbol and let Σ denote the alphabet of all these symbols. The segment, visited by the time series plot takes a symbol value from the alphabet Σ . For example, having $\Sigma = \{\alpha, \beta, \gamma, \delta\}$ in Fig. 1, a time-series $x_0 x_1 x_2 \dots$ generates a sequence of symbols in the symbol space as: $s_0 s_1 s_2 \dots$, where each $s_i, i = 0, 1, 2, \dots$, takes a symbol value from the alphabet Σ . This mapping is called symbolic dynamics as it attributes a (physically admissible) symbol sequence to the dynamical system starting from an initial state. For example, see the symbol sequence at the top right hand corner of Fig. 1.

The core assumption in the SDF analysis for construction of probabilistic finite state automata (PFSA) from symbol sequences is that the symbolic process under both nominal and off-nominal conditions can be approximated as a Markov chain of order D , called the D-Markov machine, where D is a positive integer. While the details of the D-Markov machine construction are given in Refs. [3], [13], the pertinent definitions and their implications are succinctly presented below.

Definition 3.1. (DFSA) A deterministic finite state automaton (DFSA) is a 3-tuple $G = (\Sigma, Q, \delta)$ where:

- 1) Σ is a non-empty finite set, called the symbol alphabet, with cardinality $|\Sigma| < \infty$;
- 2) Q is a non-empty finite set, called the set of states, with cardinality $|Q| < \infty$;
- 3) $\delta: Q \times \Sigma \rightarrow Q$ is the state transition map;

and Σ^* is the collection of all finite-length strings with symbols from Σ including the (zero-length) empty string ϵ , i.e., $|\epsilon| = 0$.

Remark 3.1. It is noted that Definition 3.1 does not make use of an initial state, because the purpose here is to work in a statistically stationary setting, where no initial state is required as explained by Adenis et al. [14].

Definition 3.2. (PFSA) A probabilistic finite state automaton (PFSA) is constructed upon a DFSA $G = (\Sigma, Q, \delta)$ as a pair $K = (G, \pi)$, i.e., the PFSA K is a 4-tuple $K = (\Sigma, Q, \delta, \pi)$, where:

- 1) Σ, Q , and δ are the same as in Definition 3.1;
- 2) $\pi: Q \times \Sigma \rightarrow [0,1]$ is the probability morph function that satisfies the condition $\sigma_{\sigma \in \Sigma} \pi(q, \sigma) = 1 \quad \forall q \in Q$. Denoting π_{ij} as the probability of occurrence of a symbol $\sigma_j \in \Sigma$ at the state $q_i \in Q$, the $(|Q| \times |\Sigma|)$ probability morph matrix is obtained as $\Pi = [\pi_{ij}]$.

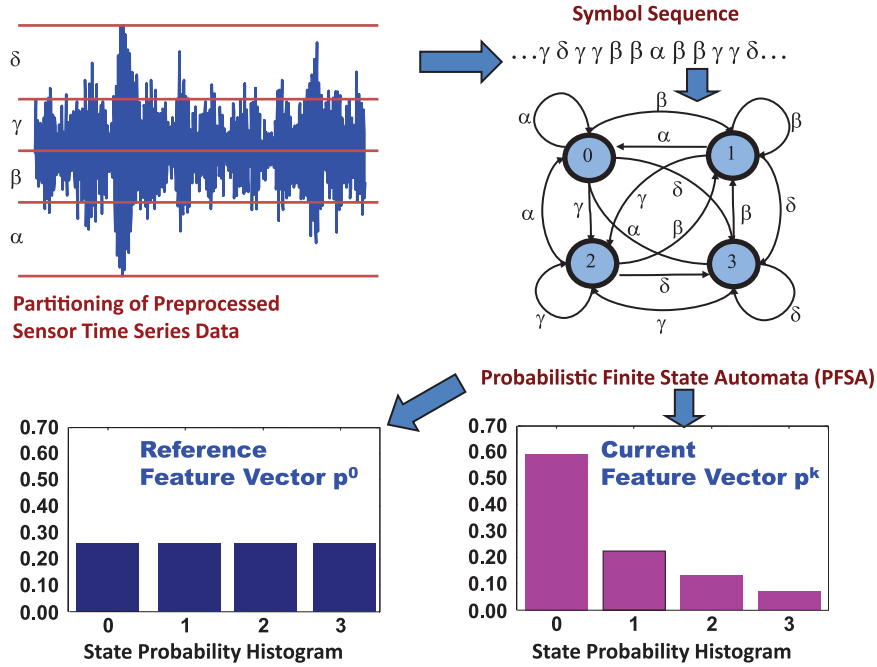


Fig. 1. Concept of symbolic dynamic filtering (SDF).

Definition 3.3. (D-Markov) A D-Markov machine [3] is a PFSA in which each state is represented by a finite history of D symbols as defined by:

- D is the depth of the Markov machine;
- Q is the finite set of states with cardinality $|Q| \leq |\Sigma|^D$, i.e., the states are represented by equivalence classes of symbol strings of maximum length D where each symbol belongs to the alphabet Σ ;
- $\delta: Q \times \Sigma \rightarrow Q$ is the state transition map that satisfies the following condition if $|Q| = |\Sigma|^D$: There exist $\alpha, \beta \in \Sigma$ and $s \in \Sigma^*$ such that $\delta(\alpha s, \beta) = s\beta$ and $\alpha s, s\beta \in Q$.

Remark 3.2. It follows from Definition 3.3 that a D-Markov chain is treated as a statistically stationary stochastic process $S = \dots s_{-1}s_0s_1\dots$, where the probability of occurrence of a new symbol depends only on the last D symbols, i.e., $P[s_n|s_{n-1}\dots s_{n-D}\dots s_0] = P[s_n|s_{n-1}\dots s_{n-D}]$.

The construction of a D-Markov machine is based on: (i) state splitting that generates symbol blocks of different lengths according to their relative importance; and (ii) state merging that assimilates histories from symbol blocks leading to the same symbolic behavior. Words of length D on a symbol sequence are treated as the states of the D-Markov machine before any state-merging is executed. Thus, on an alphabet Σ , the total number of possible states becomes less than or equal to $|\Sigma|^D$; and operations of state merging may significantly reduce the number of states [15].

Following Fig. 1 where The parameter D of the D-Markov machine is chosen to be 1, the time series at a given epoch t^k may now be used to compute the quasi-stationary probability morph matrix Π^k (see Definition 3.2). Then, Π^k is used in conjunction with the state transition map δ (see Definition 3.1), to construct the $(|Q| \times |Q|)$ quasi-stationary stochastic irreducible state-transition matrix as: $P^k \triangleq [p_{ij}^k]$, where p_{ij}^k is the probability of transition from state q_i to state q_j based on time series at epoch t^k . The corresponding state probability vector is obtained as: $p^k \triangleq [p_1^k, \dots, p_{|Q|}^k]$, where p_j^k is the quasi-stationary probability of occupying the state

$q_j \in Q$ at epoch t^k , as the (sum-normalized) left eigenvector of P^k corresponding to its (unique) unity eigenvalue.

The statistics of the time series at the epoch t^k , represented by the state transition probability matrix P^k , change to P^l at another epoch t^l . Accordingly, the state probability vector p^k changes to p^l ; thus, p^k and p^l are treated as feature vectors that are postulated to have the imbedded information on the dynamical system at the epochs t^k and t^l , respectively. The evolution of the battery dynamics is captured as the divergence of the feature vector as defined below.

Definition 3.4. (Feature Divergence) Let p^0 be the feature vector at the epoch t^0 , which is treated as a reference (e.g., full charge or healthy) condition of the battery, and let p^k be the feature vector at the current time epoch t^k . Then, the (scalar) feature divergence at an epoch t^k is expressed as:

$$m_k \triangleq d(p^k, p^0) \quad (4)$$

where $d(\cdot, \cdot)$ is an appropriate metric, while there are several choices for this metric (for example, see [3]).

The range of linearity between the feature divergence and a battery condition (e.g., SOH) is obtained as a statistical model in terms of the coefficient of determination as defined below.

Definition 3.5. (Coefficient of Determination [16]) As a measure of how well the linear least squares fit, $\hat{\theta}_k = a + b m_k$, performs as a predictor of an output θ in terms of the input m , where the scalars a and b are the intercept and slope of the linear fit, the coefficient of determination (R^2) is defined as:

$$R^2 = 1 - \frac{\sum_{i=1}^n (\theta_i - \hat{\theta}_i)^2}{\sum_{i=1}^n (\theta_i - \bar{\theta})^2} \quad (5)$$

where $\bar{\theta} \triangleq 1/n \sum_{i=1}^n \theta_i$ is the average of the output data. In this paper, $\{m_k\}$ represents a sequence of the feature divergence and $\{\theta_k\}$ is the corresponding sequence of $(1 - \text{SOH})$.

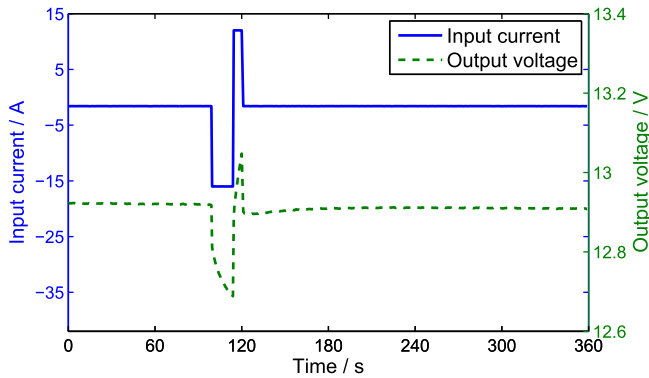
4. Results and discussion

This section presents the results of SOC and SOH estimation based on an ensemble of time series data sets of current inputs and voltage outputs. These data sets were acquired from three lead-acid batteries with similar characteristics. All batteries are of the same type: 12 V AGM VRLA with 85 Ah capacity. Battery #1 and Battery #2 are from the same manufacturer while Battery #3 is from a different manufacturer. Experiments were conducted on these batteries under two long-term (i.e., over 100 days) tests at room temperature. Two different current input cycle patterns, denoted as “Pattern I” and “Pattern II”, have been used to charge/discharge the batteries; each of these patterns simulates a real-time working condition for an electric locomotive. Fig. 2 shows a current profile consisting of a constant “hotel” load and a discharge pulse followed by a constant charge (i.e., regeneration) pulse.

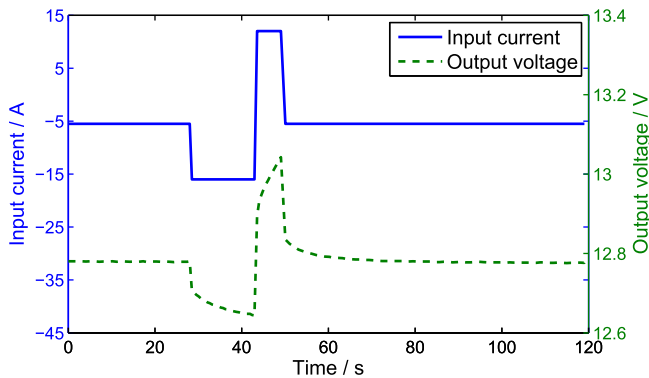
The configuration of an experiment depends on the type of current input pattern, as depicted in Fig. 3. During each test, an input pattern is repeated for 8 h, which is called one working cycle. The SOH is calibrated after every 15 (or more) working cycles. Two slow, full charge/discharge cycles have been used to measure the battery current capacity.

The parameters for SDF analysis (see Section 3) of time series data have been chosen as follows.

- The size of the symbol alphabet is chosen to be $|\Sigma| = 20$.
- The depth in the D-Markov machine is set at $D = 1$.



(a) Pattern I input current and output voltage cycle



(b) Pattern II input current and output voltage cycle

Fig. 2. Two patterns of battery input current and output voltage patterns in the experiment: (a) Pattern I – Cycle length = 360 s starting with steady discharge current of $-1.6 \text{ A}(C/53 \text{ A})$; (b) Pattern II – Cycle length = 120 s starting with steady discharge current of $-5.5 \text{ A}(C/15 \text{ A})$. Both patterns include 14 s of $-16 \text{ A}(C/5.3 \text{ A})$ discharge pulse and 6 s of $12 \text{ A}(C/7 \text{ A})$ charge pulse.

- The distance function $d(\cdot, \cdot)$ for computation of the feature divergence in Eq. (4) is chosen to be the standard Euclidean distance, i.e., $m_k = \left\| p^k - p^0 \right\| \triangleq \sqrt{\sigma_j(p_j^k - p_j^0)^2}$,

4.1. SOC estimation by SDF-based kNN regression

This subsection performs SOC estimation based on the SDF features, extracted from voltage responses during working cycles, where a k -nearest-neighbor (kNN) regression algorithm [17] is trained by the SDF features. The results, reported in this subsection, focus on experimental data with the input pattern II (see Fig. 2(b)), where the battery is charged back to full SOC during the interval between two consecutive working cycles. At different SOC levels, lead-acid battery voltage responses can be different for identical current inputs as seen in Fig. 4, where the normalized voltage outputs (with zero mean and unit variance) have different textures for inputs of the same pattern. SDF capture these subtle differences in the voltage responses and represent them as low-dimensional feature vectors. It is noted that the kNN method is among the most frequently used and simplest tools of pattern classification and regression. This algorithm recognizes the contributions of nearest neighbors, which means only local data density is taken into consideration, which is especially efficient for high data density and large data sets.

Algorithm 1. kNN regression algorithm for SOC estimation

Input: Normalized training time series data $\bar{x}_j^i \in \mathbb{R}^{1 \times n}$, $j = 1, \dots, M, i = 1, \dots, N$;
 SOC labels for training data sets $C_j^i \in [0, 1]$, $j = 1, \dots, M, i = 1, \dots, N$;
 And test time series data set $x \in \mathbb{R}^{1 \times n}$
 (where n is the length of analysis time window, M depends on analysis window, N is the total number of training data sets.)
 Output: Estimated SOC value for the time-series x

- 1 Generate features p_j^i from the time series $\{\bar{x}_j^i\}$ for each training data using SDF.
- 2 Compute the normalized test time series $\bar{x} = x - \text{mean}(x)/\text{var}(x)$.
- 3 Generate features p from the test time series $\{\bar{x}\}$ using SDF.
- 4 Find the SOC values from each training set such that $C_{\text{chosen}}^i \triangleq C_j^i$, where $j = \text{argmin} \|p_j^i - p\|$ for each $i = 1, \dots, N$.
- 5 Estimate the SOC of test time series $\hat{\text{SOC}} = \sigma_{i=1}^N C_{\text{chosen}}^i / N$.

As the physical condition of a battery deteriorates with aging, the SOC estimator is adapted to different SOH values by choosing different training sets. In this experiment, three working cycles have been randomly chosen from 15 working cycles between two consecutive SOH calibration operations, which leaves 12 remaining working cycles as the test set. In the training phase, SDF features are extracted from the training data for a certain analysis window. The analysis window consists of single or multiple successive voltage responses to input patterns. Each SDF feature is labeled with a SOC value that corresponds to the end time of the training data in the analysis window. In the testing phase, SDF features are extracted from real-time voltage outputs of the same length as the analysis window. Next, one SDF feature with the minimum Euclidean distance from the test feature is chosen from each training data set. The SOC of the test data is estimated as the average of SOC for 3 SDF features.

Fig. 5 shows the results of cross validation to assess the performance of SOC estimation based on SDF feature extraction and kNN regression. By choosing different 3 training sets from every 15 working cycles between SOH calibrations, there are 455 different training data combinations. For different choice of analysis time window at each SOH level, we compute the average estimation

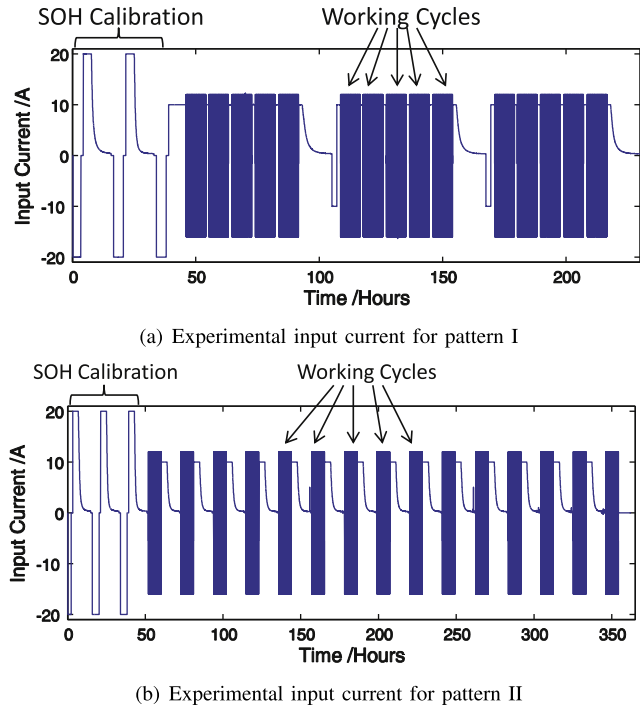


Fig. 3. Configuration of working cycles in two patterns: (a) Pattern I – 5 working cycles grouped together with a 1.5-h interval between consecutive working cycles and a 17-h interval between two consecutive groups; (b) Pattern II – single working cycles with a 13-h interval between consecutive working cycles.

errors for all training data combinations and take the mean value as the error of SOC estimation in that case. The results suggest that the SOC estimation error increases as the battery ages, and more accurate estimations can be made if the analysis window length is increased.

4.2. SOH estimation by feature divergence

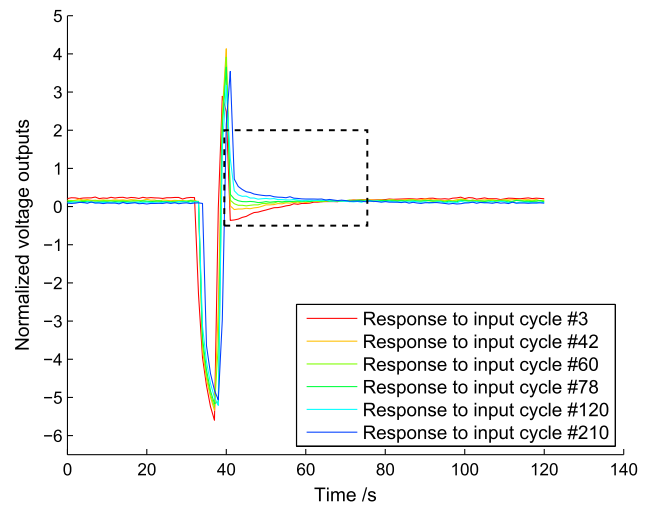
This subsection presents SOH estimation in lead-acid batteries based on the SDF features extracted from single or multiple successive voltage outputs in a working cycle (voltage responses during charging between working cycles are removed). The estimated SOH for real-time data is measured by feature divergence (see Eq. (4) in Definition 3.4) between the reference feature, extracted from the time series of the new battery (i.e., voltage outputs for first few working cycles) and the feature vector, extracted from the current time series, which has the same length as the reference pattern.

The six plates in Fig. 6 present the results of SOH estimation for three batteries, where the time series for each battery was acquired over a testing period of 40 h (i.e., 5 working cycles). It is observed in the top three plates of Fig. 6 that there exists an approximately linear relationship between feature divergence and SOH, which is determined by linear regression. In Fig. 7, this linearity is measured by the coefficient of determination (see Eq. (5) in Definition 3.5), which indicates how well data points fits a line model constructed in least squares sense. The inverse of this relationship is used to obtain the estimated SOH from the computed feature divergence of the test feature from the training reference feature. The choice of the testing time period depends on the relationship between the feature divergence and the estimated SOH. As the testing period is increased, the range of linearity between change of true SOH value and feature distance is increased.

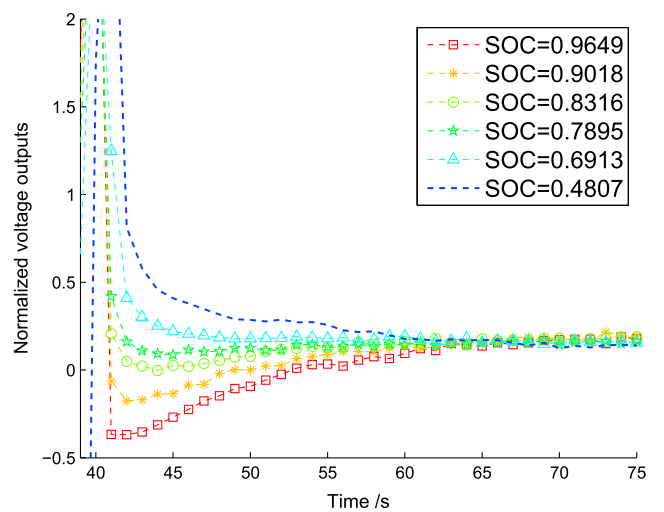
The results show that the SDF features from all three experimental data sets are capable of capturing the characteristics of battery aging. Furthermore, the feature divergence remains within the same range of scale across all data sets from three batteries. It can be concluded from this observation that the feature divergence remains independent of the type of discharge pattern applied, as seen in Fig. 8.

4.3. Computational costs

This subsection presents a statement of the computational costs (i.e., execution time and memory requirement) of the SDF algorithm for battery parameter estimation. In this paper, all results have been generated on a single core 3.6 Ghz CPU with 12 GB memory. At the SOC estimation stage, the execution time for SDF feature extraction is ~0.6 ms for time series data that were collected over 2 min at a sampling frequency of 1 hz with an increment of 0.4 ms for every additional data over next 2 min. As for SOH estimation, the cost of SDF feature extraction is also proportional to the time series length; it takes ~0.1 s for every

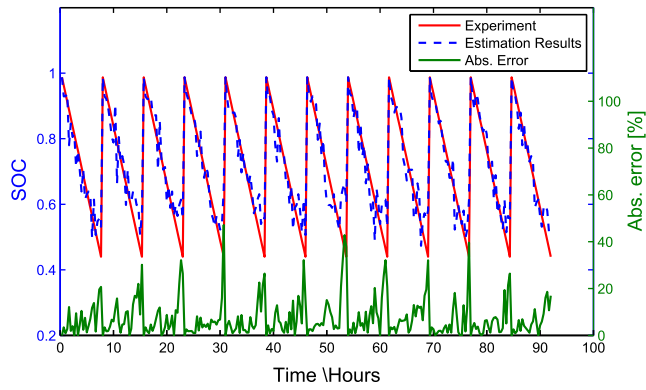


(a) Output voltage at different input cycles

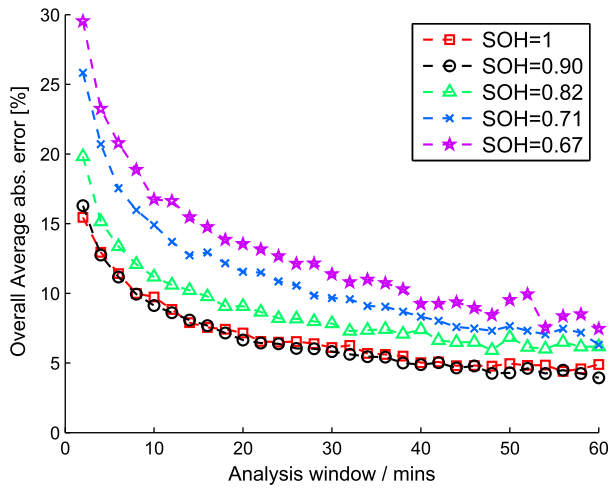


(b) Detail of the dashed rectangle in (a)

Fig. 4. Voltage responses to input Pattern II at SOH = 0.8179. The voltage response is different for charging and discharging as battery SOC drops.



(a) Average absolute error = 6.15%



(b) Average estimation errors at different battery conditions

Fig. 5. Results of cross validation for SOC estimation: (a) SOH = 0.8853 and analysis window = 20 min; (b) Estimation errors for different analysis window lengths at different SOH.

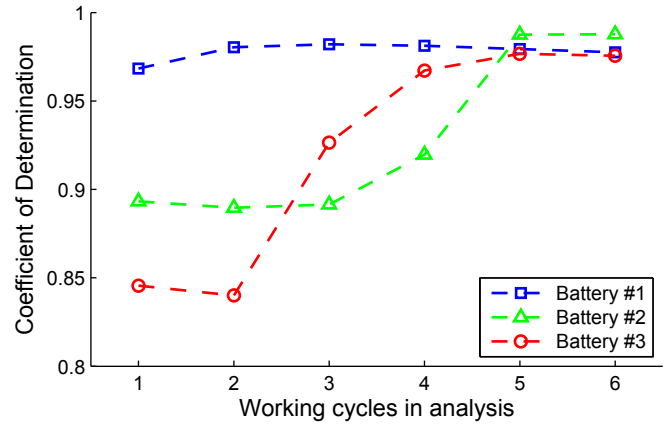
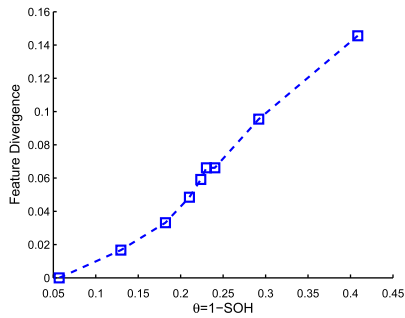
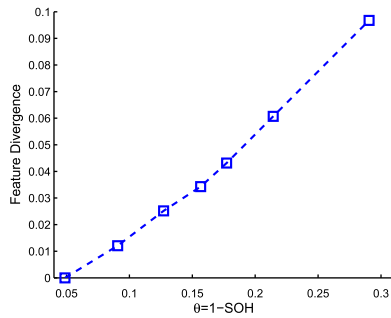


Fig. 7. Relationship between feature divergence and coefficient of determination for SOH for different analysis length. [Note: Coefficient of determination (R^2) is a real number between 0 and 1; higher the value of R^2 , better is the linear relation (see Eq. (5) in Definition 3.5).

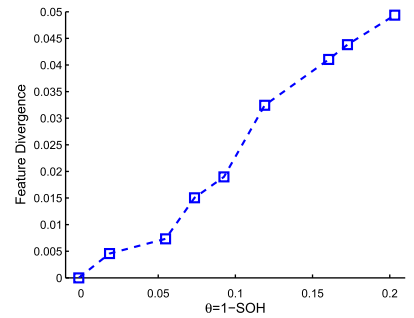
working cycle (i.e., 8 h of output voltage response). Since 5 working cycles of analysis window have been chosen for feature vector generation, the corresponding execution time is ~0.5 s. In summary, the execution time of SDF feature extraction for SOC estimation is in the order of milliseconds, and it is in the order of deciseconds for SOH estimation because of longer observation period. In real applications, such as hybrid electric vehicles, the sampling frequency of current/voltage is much higher than that used in this paper (1 Hz). As discussed in the last subsection, the performance of the proposed algorithm depends on the length of data in analysis. An appropriate choice of the data length depends on the battery system dynamics that also determine the sampling frequency of data acquisition.



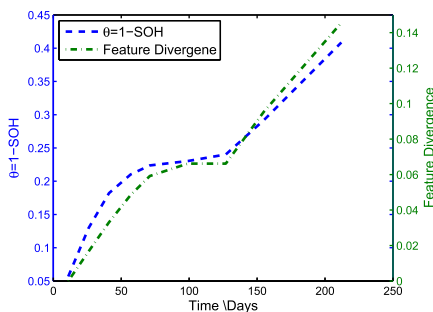
(a) SOH vs feature divergence, battery #1



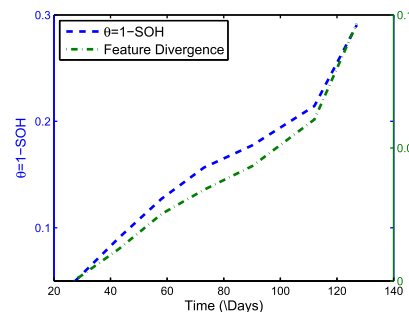
(b) SOH vs feature divergence, battery #2



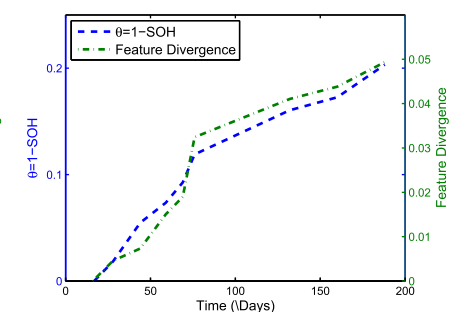
(c) SOH vs feature divergence, battery #3



(d) SOH time history of battery #1



(e) SOH time history of battery #2



(f) SOH time history of battery #3

Fig. 6. Results of SOH estimation for three batteries.

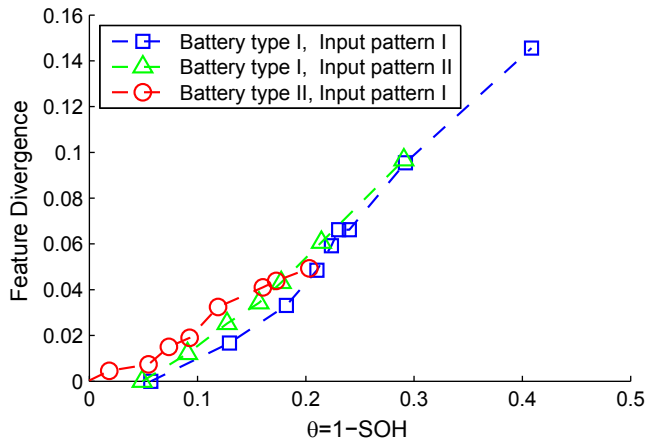


Fig. 8. Feature divergence (see Eq. (4) in Definition 3.4) versus SOH for three test cases.

5. Summary, conclusions, and future work

This paper presents a dynamic data-driven method for real-time estimation of SOC and SOH in lead-acid batteries, as an alternative to model-based methods. The proposed estimation method is built upon the concepts of symbolic dynamic filtering (SDF) [3] and kNN regression [17]. The power of the proposed method is its capability of real-time execution on in-situ computers (e.g., at sensor nodes of individual battery systems), and its efficacy has been validated with experimental time series data from three lead-acid batteries. Future research to accelerate the acceptance of the proposed method of battery SOC and SOH estimation in practice includes the following:

- Extension of the proposed method for SOC and SOH estimation with time series of synchronized input/output pairs under both periodic oscillatory and transient operating conditions.
- Extension of the SDF analysis with $D > 1$ in D-Markov machines to accommodate longer memory of the voltage response.

- Compensation for battery temperature effects on SOC and SOH estimation and battery performance prediction.
- Validation of the proposed method on other types of batteries (e.g., lithium-ion and Ni-MH) and different discharge or charge cycle patterns.
- Usage of the proposed dynamic data-driven method for estimation of “reversibility of capacity loss” in aged lead-acid batteries.

References

- [1] B. Bhangu, P. Bentley, D. Stone, C. Bingham, Veh. Technol. IEEE Trans. 54 (3) (2005) 783–794.
- [2] S. Santhanagopalan, R. White, in: “State of charge estimation for electrical vehicle batteries,” in Control Applications, 2008. CCA 2008. IEEE International Conference on., IEEE, 2008, pp. 690–695.
- [3] A. Ray, Signal Process. 84 (July 2004) 1115–1130.
- [4] S. Sonti, E. Keller, J. Horn, A. Ray, J. Dyn. Syst. Meas. Control 136 (2) (2014) 024505.
- [5] X. Jin, K. Mukherjee, S. Gupta, A. Ray, Pattern Recognit. 44 (July 2011) 1343–1356.
- [6] C.D. Rahn, C.-Y. Wang, Battery Systems Engineering, John Wiley, 2012.
- [7] A. Delaille, M. Perrin, F. Huet, L. Hernout, J. Power Sources 158 (2) (2006) 1019–1028.
- [8] H. Blanke, O. Bohlen, S. Buller, R. De Doncker, B. Fricke, A. Hammouche, D. Linzen, M. Thele, D. Sauer, J. Power Sources 144 (2) (2005) 418–425.
- [9] T. Okoshi, K. Yamada, T. Hirasawa, A. Emori, J. Power Sources 158 (2) (2006) 874–878.
- [10] C. De Oliveira, M. Lopes, J. Power Sources 138 (1) (2004) 294–300.
- [11] C. Bose, F. Laman, in: “Battery State of Health Estimation Through coup de fouet,” In Telecommunications Energy Conference, 2000. INTELEC. Twenty-second International, IEEE, 2000, pp. 597–601.
- [12] P. Pascoe, H. Sirisena, A. Anbuky, in: “Coup de fouet based vrla Battery Capacity Estimation,” In Electronic Design, Test and Applications, 2002. Proceedings. The First IEEE International Workshop on, IEEE, 2002, pp. 149–153.
- [13] V. Rajagopalan, A. Ray, Signal Process. 11 (November 2006) 3309–3320.
- [14] P. Adenis, Y. Wen, A. Ray, Math. Control Signals Syst. 23 (1) (January 2012) 281–310.
- [15] P. Adenis, K. Mukherjee, A. Ray, in: “State splitting and state merging in probabilistic finite state automata,” in American Control Conference, San Francisco, CA, USA, June–July 2011, pp. 5145–5150.
- [16] C. Rao, Linear Statistical Inference and its Applications, vol. 22, Wiley. com, 2009.
- [17] C. Bishop, Pattern Recognition, Springer, New York, NY, USA, 2006.